# Study on the Weld-Bonding Process Optimization and Mechanical Performance of Aluminum Alloy Joints

Mingfeng Li[1,2] · Yanjun Wang[1] · Zhen Niu[3] · Shanglu Yang[1,4]

## Abstract

The 5754 aluminum alloy has been widely used in the automotive industry to reduce the weight of vehicles. The weld-bonding (WB) process comprising resistance spot welding and adhesive bonding processes effectively improves the mechanical properties of joints. However, it is still a great challenge in the WB process to obtain high-quality and defect-free nuggets of aluminum alloys. In this study, the parameters of the WB process are optimized and the mechanism of generation of defects during WB is analyzed. The results show that the welding parameters have a significant effect on the nugget sizes, among which the welding current plays the most important role. The residual adhesive can easily cause defects during welding, e.g., expulsion and porosity in the nugget. This can be effectively avoided by optimizing the welding parameters. In addition, the gas in the joints is effectively reduced by adding an appropriate preheating pulse prior to welding, thus lowering the damage degree of the adhesive layer. As a result, welded joints with better weld nugget quality and more stable mechanical properties are obtained.

**Keywords** Aluminum alloy · Weld bonding · Process optimization · Mechanical performance

## Abbreviations

| | |
|---|---|
| ANOVA | Analysis of variance |
| BIW | Body-in-white |
| E/W | Electrodes/workpieces |
| RSW | Resistance spot welding |
| S/N | Signal-to-noise ratio |
| WB | Weld bonding |

## 1 Introduction

Lightweight vehicles can effectively improve fuel efficiency, conserve energy, and reduce emissions. The use of a lightweight alloy is one of the most effective ways to reduce the weight of vehicles [1–4]. Aluminum alloys are some of the most favored materials for body-in-white (BIW) production owing to their advantages, such as low density, high specific strength, good processability, and recyclability [5, 6]; these alloys mainly include non-heat-treatable 5 series aluminum alloys (Al–Mg) and heat-treatable 6 series aluminum alloys (Al–Mg–Si) [7], in which the former are commonly used for body structures and internal panels, e.g., 5754 [8], and the latter are used for inner and outer panels, bumpers, etc. [9].

Presently, many processes have been used to join automotive material parts [1, 4, 6, 10], e.g., resistance spot welding (RSW), laser welding, friction stir welding, self-piercing riveting, flow drill screws, and friction stir blind riveting. Of these, RSW is the most important joining process for BIW manufacturing owing to its easy automation, high production efficiency, and low cost [5, 11, 12]. In a typical BIW process, there are about 4000–5000 RSW joints [9, 13, 14]. Since many parameter variables are involved in the RSW process, which is often used for high-volume automobile body production, it is tough to ensure that all the welds have consistent weld quality. Furthermore, stress is highly concentrated in the areas surrounding the spot-welded joints, which in turn reduces the static strength and decreases the fatigue performance of the weld [15].

✉ Shanglu Yang
yangshanglu@siom.ac.cn

1 Shanghai Institute of Optics and Fine Mechanics, Chinese Academy of Sciences, Shanghai 201800, China

2 University of Chinese Academy of Sciences, Beijing 100049, China

3 Beijing Benz Automotive Co., Ltd, Beijing 100049, China

4 Center of Materials Science and Optoelectronics Engineering, University of Chinese Academy of Sciences, Beijing 100049, China

Weld bonding (WB) is a process combing welding and adhesive bonding and has been increasingly used in the automotive industry to improve joint performance because it has many advantages, such as optimal mechanical properties, anti-aging performance, and sealing performance [16–18]. In the past few years, many studies have been performed and have focused on the effects of the adhesive and process parameters on joint performance. However, these studies mainly focused on the joining of steels [19–21]. Costa et al. [17] joined interstitial free steels using the WB process and found that the tensile shear strength of the joint was higher than that of the RSW joint. Further, the mechanical properties of the joints were obviously affected by the thickness of the adhesive layer. Martensitic stainless steel was joined using the WB process by Pouranvari et al. [22]. They claimed that the peak load and ductility of the weld-bonded joints with larger nugget sizes resulted from the higher contact resistances caused by the residual adhesives, which were obviously higher than that of the RSW joint. Moreover, the WB process was also used in other works to join other steels, e.g., austenitic stainless steel [21], low-carbon steel [23], dual-phase steel [24], and high-strength steel [25].

When welding aluminum alloys, high welding currents are usually needed to achieve sufficient nugget sizes, owing to the high conductivity and high thermal conductivity [26] of the alloy, which easily cause welding defects, such as expulsion and porosity. When joining aluminum alloys using the WB process, the residual adhesive layer between the workpieces show increase of contact resistance, resulting in more expulsion. At low temperatures, the fluidity of the adhesive layer is poor, which leads to the residual adhesive layer in welding zone and finally resulting in extremely high contact resistance and the occurrence of the "blasting gun" effect. Khan et al. [27–29] studied the influences of surface roughness, curing time, and welding parameters on the tensile shear load of the 6061 Al weld-bonded joints. They reported that the contact resistance and heat generation were altered by the presence of the adhesive layer, thus greatly influencing the nugget size and the width of heat-affected zone. A numerical model was established by Pereira et al. [30] to analyze the fatigue performance of the WB joints between 6082 Al samples using double component epoxy adhesive. Their results showed that the fatigue strength of the weld-bonded joints was much higher than that of the RSW welds, as determined by the bonding width of the adhesive layer.

In this work, WB experiments were designed between 2-mm-thick 5754 aluminum alloys based on the orthogonal experiment. The influence of the WB parameters on the nuggets and mechanical performance of the joints was analyzed, and the generation mechanism of defects and problems during the WB process were explored. Finally, the WB process parameters were optimized based on the orthogonal experiments to obtain joints with improved and stable quality.

## 2 Experimental Materials and Methods

### 2.1 Experimental Setup

The 5754 Al alloy with the thickness of 2 mm and high-strength epoxy (1468LV epoxy resin) adhesive were used in this study. The chemical composition of the Al alloy is listed in Table 1. The welding was performed on a medium-frequency direct current welding system equipped with an OBARA gun, a SIV37 controller, and a FANUC robot, as shown in Fig. 1. Cr–Zr–Cu electrodes were used in this work, which are spherical with a radius of curvature of 100 mm and a tip-face diameter of 10 mm.

Prior to welding, the Al sheet was cut into workpieces with dimensions of 127 mm × 38.1 mm, and the surfaces of the pieces were cleaned with acetone to remove oil and contaminants. A uniform adhesive layer of thickness around 0.2 mm was then applied on the sheet surface at the overlap area with dimensions of 38.1 mm × 25 mm, as shown in Fig. 2. The squeeze time and holding time during welding were 300 and 50 ms, respectively. After welding, the adhesive was cured for 25 min in an isothermal baking oven at a temperature of 170 °C.
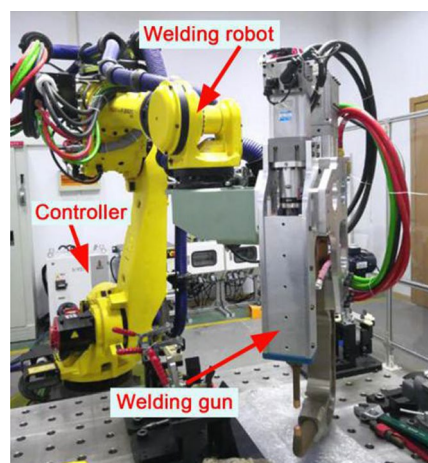


**Fig. 1** Resistance spot welding system

**Table 1** Chemical composition of 5754 aluminum alloy (wt.%) [31]

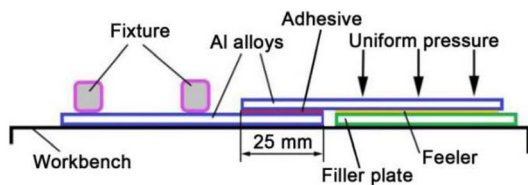| Si | Cu | Mn | Fe | Mg | Ti | Cr | Zn | Al |
|------|------|------|------|-----------|------|------|------|------|
| 0.40 | 0.10 | 0.50 | 0.40 | 2.60–3.60 | 0.15 | 0.30 | 0.02 | Bal. |

**Fig. 2** Schematic of controlling adhesive layer thickness

**Table 2** Factors and levels of orthogonal experiments

| Factor | Label (unit) | Level 1 | Level 2 | Level 3 | Level 4 |
|---|---|---|---|---|---|
| Welding current | $I$ (kA) | 24 | 26 | 28 | 30 |
| Welding time | $t$ (ms) | 90 | 120 | 150 | 180 |
| Welding pressure | $F$ (kN) | 4.0 | 4.5 | 5.0 | 5.5 |

Force–displacement curves were obtained from the tensile shear test of the joints using a universal testing machine (UTM5015) with a stroke rate of 3 mm/min. The filler plates with sizes of 40 mm×38.1 mm×2 mm were simultaneously attached to both ends of the specimens, thereby minimizing the additional bending during tensile tests. An ultra-depth metallurgical microscope (VHX-6000) was used to observe the cross-sectional and failure morphologies.

## 2.2 Orthogonal Experiment

The Taguchi's orthogonal array was used to minimize the number of experiments. For the three main factors affecting welding, i.e., welding current, welding time, and welding pressure, four levels for each factor were applied on the basis of our previous experiments, as shown in Table 2. The Taguchi's orthogonal array of $L_{16}(4^3)$, consisting of 16 groups of experiments, was selected as shown in Table 3. The weld nugget areas $S$ and the tensile shear forces $F_\tau$ of the joints were selected as the response values in the orthogonal experiments. Three replicas were tested for each parameter group, and the average value was calculated.

## 3 Results and Analyses

## 3.1 Analysis of the Effects of Welding Parameters

In order to evaluate the influences of the three main factors on the nugget area and mechanical properties of WB joints, the analyses of the Taguchi experiment were performed using Minitab 16. To determine the optimal combination of welding parameters, the signal-to-noise ratio (S/N) was used as the stability evaluation index for the nugget size and joint mechanical properties [32]. Therefore, the larger-the-better characteristic of Eq. (1) [33] was selected to calculate S/N.

**Table 3** $L_{16}(4^3)$ orthogonal array and experimental results

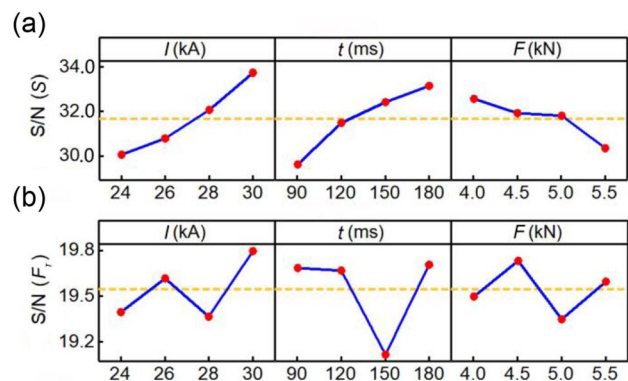| No. | Factor | | | Experimental result | |
|---|---|---|---|---|---|
| | $I$ (kA) | $t$ (ms) | $F$ (kN) | $S$ (mm$^2$) | $F_\tau$ (kN) |
| 1 | 24 | 90 | 4.0 | 28.1 | 9.5 |
| 2 | 24 | 120 | 4.5 | 29.9 | 9.5 |
| 3 | 24 | 150 | 5.0 | 35.0 | 8.3 |
| 4 | 24 | 180 | 5.5 | 35.0 | 10.1 |
| 5 | 26 | 90 | 4.5 | 28.6 | 10.2 |
| 6 | 26 | 120 | 4.0 | 39.4 | 9.5 |
| 7 | 26 | 150 | 5.5 | 29.0 | 9.4 |
| 8 | 26 | 180 | 5.0 | 43.8 | 9.2 |
| 9 | 28 | 90 | 5.0 | 31.8 | 9.7 |
| 10 | 28 | 120 | 5.5 | 35.5 | 9.5 |
| 11 | 28 | 150 | 4.0 | 49.2 | 8.7 |
| 12 | 28 | 180 | 4.5 | 46.7 | 9.3 |
| 13 | 30 | 90 | 5.5 | 32.6 | 9.2 |
| 14 | 30 | 120 | 5.0 | 47.4 | 10.0 |
| 15 | 30 | 150 | 4.5 | 60.8 | 9.8 |
| 16 | 30 | 180 | 4.0 | 59.8 | 10.1 |



**Fig. 3** Main effects plots of S/N ratios: **a** nugget areas; **b** tensile shear forces

$$S/N \text{ (Larger - the - better)} = -10 \lg \left[ \frac{1}{n} \sum_{i=1}^{n} \frac{1}{y_i^2} \right] \quad (1)$$

where $n$ and $y_i$ are the number of measurements and measured characteristic values, respectively.

Figure 3 shows the relationships between the various factors and nugget area or tensile shear force. As shown, the nugget area increases with the increment of welding current and welding time but decreases with the increase in pressure (refer to Fig. 3a). According to Joule's law, $Q = I^2 R t$ (where $I$ is the welding current, $t$ is the welding time, and $R$ is the total resistance), the total Joule heat during welding increases with increasing welding current and time, resulting in rapid growth of the weld nugget. When increasing the

welding pressure, the adhesive layer can be expelled better, resulting in a larger contact area between the workpieces, thus lowering the contact resistance and current density as well as reducing the Joule heat for weld initiation. Therefore, the weld nugget area decreases with the increase in welding pressure. To determine the influence of the welding parameters on tensile shear force, as shown in Fig. 3b, the nonlinear relationships are observed. With the main effects plots of the S/N ratios, a good set of values for the welding parameters was achieved: $I = 30$ kA, $t = 150$ ms, $F = 4.5$ kN. However, further experimental results show that adhesive was seriously damaged during WB process. As a consequence, the welding parameters were further optimized in Sect. 4.

Analysis of variance (ANOVA) can reveal the significance of a factor or factor interactions on the responses [33, 34]. Table 4 presents the ANOVA results of the orthogonal experiments. The larger the $F$ value, the better is the fitting degree of the fitting equation, and more significant influence on the response can be achieved [34]. A confidence level of 95% was set during the ANOVA, indicating that the effect of the factor is significant at a $p$ value less than 0.05 [33]. As shown in Table 4, the three main welding parameters have significant effects on the nugget area, and the welding current is the most significant factor, followed by the welding time and pressure, which is the least significant factor. However, the welding parameters have little effect on the mechanical properties of the joints, whose $p$ value of all the factors is much larger than 0.05, from the gas defects caused by the decomposition of the adhesive or expulsion during welding, thus causing the poor mechanical properties of the joints.

## 3.2 Generation Mechanism of Expulsion

In this work, around 95.8% of the welds showed expulsion. Therefore, it is necessary to understand the expulsion during the WB process. The distribution of the adhesive layer at the faying interface after the squeeze stage is shown in Fig. 4. A thin layer of the residual adhesive in the circular region with a diameter of about 4 mm is observed, while many metallic contact points with little adhesive are observed at the regions with diameters ranging from 4 mm to 6 mm, indicating that
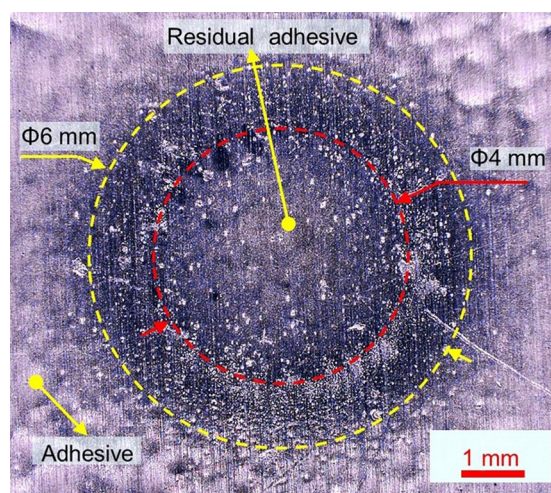


**Fig. 4** Distribution of adhesive layer after squeezing prior to curing treatment

this annular region has a better contact state before welding. As shown, the regions with a diameter of larger than 6 mm are adhesive. For the spherical electrodes used in this study, the interfacial pressures between the electrodes/workpieces (E/W) were not uniform. Rashid et al. [35] claimed that the pressure gradually increased from the center to the outside and reached a maximum at the annular region, at a diameter of about 4.5 mm, when using the electrodes with a radius of curvature of 50 mm. The pressure at the faying interface between the workpieces had similar variations to that on the E/W interface. The lower interfacial pressure at the center of the E/W and workpieces/workpieces (W/W) interfaces caused some residual adhesive layers, as shown in Fig. 4.

A schematic of the splash generation process is shown in Fig. 5. Prior to welding, the two workpieces were isolated by the adhesive layer (refer to Fig. 5a). As the electrode force increased, a large amount of adhesive was squeezed out from the welding zone (refer to Fig. 5b). However, some residual adhesive is still observed at the center region of the joint, caused by the low interfacial pressure at the center and the viscous characteristics of the adhesive layer, causing poor contact between the sheets. However, a good contact was established in the ring region with little residual adhesive

**Table 4** Results of ANOVA

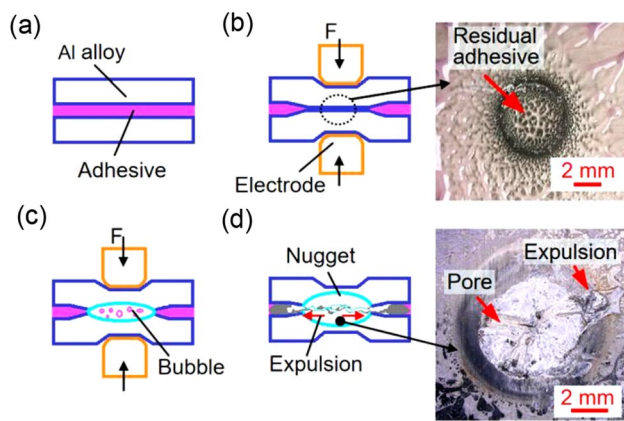| Item | Degrees of freedom | ANOVA of nugget area | | | | | ANOVA of tensile shear force | | | | |
|---|---|---|---|---|---|---|---|---|---|---|---|
| | | Seq SS | Adj SS | Adj MS | $F$ value | $P$ value | Seq SS | Adj SS | Adj MS | $F$ value | $P$ value |
| $I$ | 3 | 759.39 | 759.39 | 253.13 | 19.12 | 0.002 | 0.575 | 0.575 | 0.192 | 0.61 | 0.635 |
| $t$ | 3 | 599.11 | 599.11 | 199.70 | 15.08 | 0.003 | 1.085 | 1.085 | 0.362 | 1.14 | 0.405 |
| $F$ | 3 | 269.24 | 269.24 | 89.75 | 6.78 | 0.024 | 0.340 | 0.340 | 0.113 | 0.36 | 0.786 |
| Error | 6 | 79.43 | 79.43 | 13.24 | | | 1.900 | 1.900 | 0.317 | | |
| Total | 15 | 1707.18 | | | | | 3.900 | | | | |

**Fig. 5** Schematic of expulsion generation and typical fractographies of weld-bonded joints: **a** alignment and clamping; **b** squeezing; **c** welding; **d** resulting joint



**Fig. 6** Failure morphologies of the weld-bonded joints: **a–d** welding parameters corresponding to trial nos. 15, 8, 11, and 4 in Table 3, respectively

layer, resulting in a large local current density during welding and higher resistance heat, causing expulsion in the early welding stage. Meanwhile, the adhesive was decomposed into gases by resistance heat, and the gases accumulated and rapidly expanded, generating porosities (refer to Fig. 5c). During the welding process, a corona bond was formed around the nugget due to plastic deformation and strong recrystallization of the base material under the action of thermal and mechanical effects, preventing or postponing the occurrence of expulsion [36]. However, the growth speed of the nugget was faster than that of the corona bond, easily breaking through the corona bond by the liquid metal and causing expulsion. On the other hand, the gap between the two workpieces is larger than that during RSW owing to the residual adhesive, delaying the increase in effective contact area between the workpieces and thus higher local current density, promoting expulsion. As a result, large gas pores and expulsions are generated in the nugget (refer to Fig. 5d).

### 3.3 Failure Morphologies and Mechanical Properties of Joints

Obviously, the mechanical properties of the weld-bonded joints were mainly determined by both the weld quality and the adhesive bonding performance. The larger the weld nugget size, the higher is the strength. However, the existence of the welding defects weakens the strength of WB joints [37]. The adhesive bonding quality was also determined by the bonding width and the properties of the adhesive. During welding, the adhesive between the two workpieces increased the nonconformity of the contact state, affecting the formation and growth of the weld nugget and thus the joint performance.

The typical failure morphologies in orthogonal experiments are shown in Fig. 6. It can be seen from Fig. 6a that
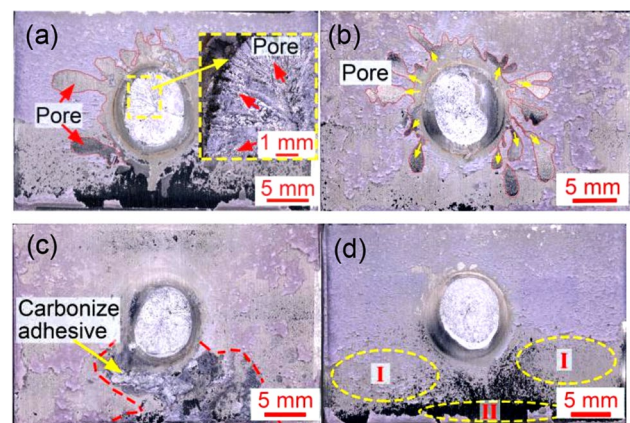
there are grooves on the nugget caused by the ejection of gas, destroying the integrity of the nugget. Furthermore, the adhesive layer around the weld also decomposed into gases at high temperatures. When a large amount of gases migrate into the adhesive layer, the adhesive layer will suffer from gas extrusion to form pores, which reduce the effective bonding area (refer to Fig. 6a, b). Expulsion is also a key factor in destroying the bonding of the adhesive (Fig. 6c). The molten metal was ejected from the weld nugget to burn and carbonize the surrounding adhesive layer, resulting in failure of the adhesive bonding in this region. The amount and distribution of the residual adhesive in each weld were random, causing different amounts of gases and expulsions under the same heat input, which resulted in an unobvious but significant effect of the welding parameters on the tensile shear forces.

The failure modes of the adhesive layer in the WB joints are usually divided into three types: cohesive failure, interface failure, and mixed failure. The cohesive failure indicates that the cohesive strength of the adhesive layer is less than that of the adhesive strength between the substrate surface and adhesive layer. The interface failure is due to poor interfacial bonding strength between the adhesive layer and workpiece. The mixed failure is a failure mode that coexists with interface failure and cohesive failure [38, 39]. The region I and region II marked in Fig. 6d are cohesive failure and interface failure, respectively. In this experiment, the main fracture mode of the adhesive layer is cohesive failure (Fig. 6b), which indicates that the adhesive layer has a strong bonding effect on the substrate. Nevertheless, there are interface fractures in a few joints, as shown in Fig. 6a, d. Since the factors affecting the failure mode of the adhesive layer, such as curing time, roughness of the workpiece surface, and content of the adhesive layer, are controlled almost uniformly, the most important cause for the local interface
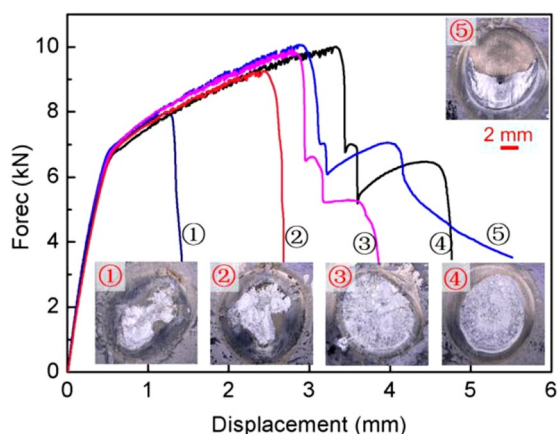
**Fig. 7** Force–displacement curves and failure surfaces of the welded joints: ①–⑤ welding parameters corresponding to trial nos. 3, 7, 16, 4, and 15 in Table 3, respectively

fracture of the adhesive layer is the expulsion of the nugget. The bonding strength of the adhesive layer was almost lost when carbonized by high-temperature liquid metal. As shown in Fig. 6c, the region after carbonization exhibits interface failure on the other side of the fracture.

The force–displacement curves of the typical weld-bonded joints are plotted in Fig. 7. As shown, two types of curves are observed for the welded joints, i.e., the rapid rupture at the tensile shear force is larger than the maximum value (① and ② in Fig. 7), and a platform appearing at the tensile shear force drops to a certain value (green ellipses on curves ③, ④, and ⑤ in Fig. 7). For the WB joint, the maximal shear stress was distributed at the edge of the overlap region, while the stress at the center of the overlap region was the lowest [40]. During the tensile shear tests, the joint rotated owing to the eccentricity of the loading, causing tearing at the edge of the overlap region, then gradually advancing to the center area, and finally breaking the adhesive layer. For the nugget corresponding to the curves ① and ②, serious expulsion affected the bonding performance of adhesive layer, lowering the resistance capacity of the joint for shear load, which caused breaking of the nugget and the adhesive layer simultaneously under low external load. For the weld corresponding to the curve ⑤, no expulsion is observed, and a nugget pull-out failure was generated, owing to the ability to bear large tensile loads after the failure of the adhesive layer.

## 4 Optimization of the Process Parameters

When joining the aluminum alloys using the WB process, the adhesive can be easily decomposed into gases at high temperatures, forming welding defects and destroying the integrity of the weld nugget. Moreover, adhesive

easily remained on the interface between the workpieces, increasing local contact resistance and current density, thus aggravating the occurrence of expulsion, deteriorating joint properties, and lowering its stability. Though good joining property was achieved using the WB process with the parameters optimized by Taguchi's experiment for Al, the expulsion during welding and the gas pores in the joint were both serious. To avoid the existence of residual adhesive on workpieces interfaces during welding to reduce expulsion and welding defects, e.g., gas pores, the RSW process of the WB process should be optimized based on the results of Taguchi's experiments.

As analyzed above, the increasing welding pressure would increase the interfacial pressure and thus achieve higher pressure at the center of the contact region, contributing to expelling the adhesive from the welding zone and thus reducing the residual adhesive. The contact resistance and local current density of the joint are reduced owing to the decrease in the residual adhesive, avoiding or delaying the occurrence of expulsion. As shown in Fig. 3a, a larger current generates a larger nugget; however, over-large currents will bring about excessive heat input, causing expulsion. To ensure the nugget size and reduce expulsion, a shorter welding time was selected to reduce the heat input. Moreover, a preheating pulse with low current was added to promote the expelling of the adhesive from the welding zone, thus increasing the effective contact area between workpieces and lowering the intensity of the heat input during welding. Table 5 shows the optimized welding parameters. The welding pressure was increased to 5.5 kN, and the welding time was decreased to 150 ms. A current of 10 kA was applied for the preheating pulse with different preheating times.

Figure 8 shows the failure morphologies of the typical joints achieved using the optimized welding parameters. As shown, the failure mode of welding spot is interface failure, and the adhesive layer is cohesive failure. Refer to Fig. 8a, obvious carbonized adhesive in the center of the nugget and some gas pores in the adhesive layer could be observed in the WB-I joint. After 100 ms of preheating pulse, the nugget on the failure surface is relatively full, and no serious nugget exclusion is observed. However, there are still some pores formed by gas extrusion in the adhesive layer surrounding the nugget, caused by thermal decomposition of the adhesive

**Table 5** Optimized parameters for WB process

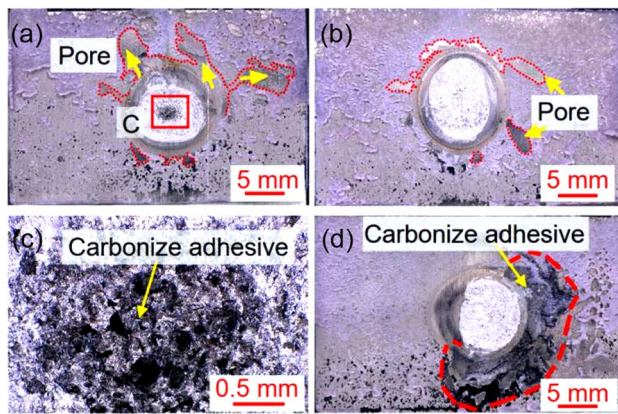| No. | Preheating current (kA) | Preheating time (ms) | Welding current (kA) | Welding time (ms) | Welding Pressure (kN) |
|---|---|---|---|---|---|
| WB-I | | | 30 | 150 | 5.5 |
| WB-II | 10 | 100 | 30 | 150 | 5.5 |
| WB-III | 10 | 200 | 30 | 150 | 5.5 |

**Fig. 8** Fractographies of the joints achieved with the optimized parameters: **a**, **b** and **d** are failure surfaces of WB-I, WB-II, and WB-III joints, respectively; **c** is a local enlargement in (**a**)

around the weld (refer to Fig. 8b). Serious expulsion occurs in the weld nugget shown in Fig. 8d, resulting in a large carbonization failure area of the surrounding adhesive layer at the preheating time of 200 ms.

The distribution of the uncured adhesive layer after preheating pulse is shown in Fig. 9. As shown, some adhesive that aggregates into a granular form remains in the center area of the solder joint, and the adhesive layer is obviously less and discontinuous resulting from the thermal decomposition of some adhesive after preheating. Moreover, preheating improves the fluidity of the adhesive layer and facilitates the flow of undecomposed adhesive to the outer of the weld, which further increases the area of direct intermetallic contact between electrodes and reduces the contact resistance. As shown in Fig. 9a, very small nuggets first form in the region with a diameter of about 6 mm, verifying that the area is a direct contact region between sheets after squeezing. Moreover, preheating softens the sheets, thus lowering the intensity of heat input during welding and reducing the occurrence of expulsion. As a result, serious expulsion is not observed on the failure surface of the WB-II joints. As the preheating time reaches 200 ms, the adhesive is completely decomposed and expelled out, and thus, no residual adhesive is observed in the failure surface of the WB-III joints (refer to Fig. 9b).

Figure 10 shows the cross-sectional morphologies of the weld-bonded joint achieved using the optimized parameters listed in Table 5. As shown, many gas pores could be observed in the nugget with or without preheating pulse, caused by the hydrogen gases from the hydrated oxide film of Al sheet. In addition, the gas formed through decomposing the adhesive at high temperature will also lead to pores. Compared to the WB-III weld shown in Fig. 10c, the WB-I and WB-II own a larger nugget penetration (refer to Fig. 10a, b). The residual adhesive at welding zone caused
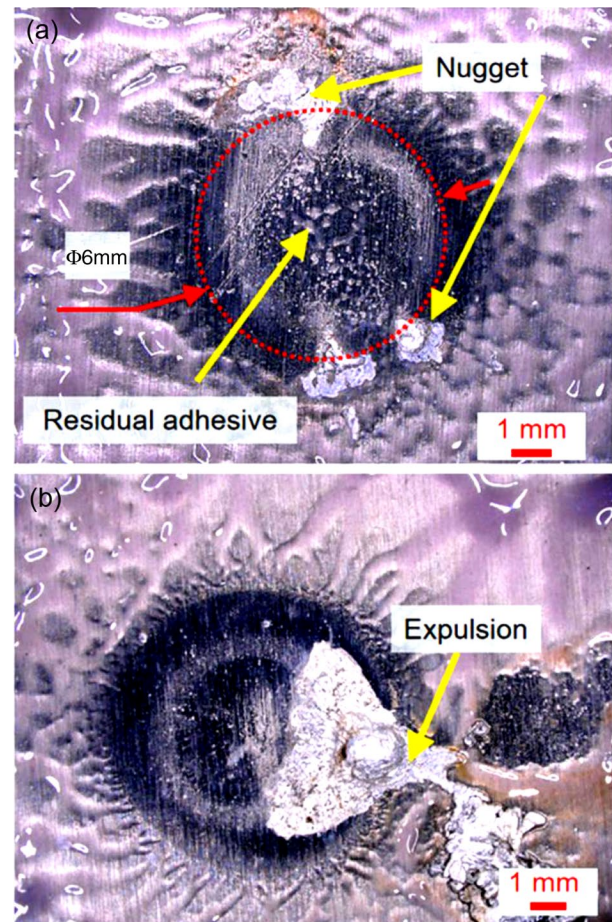


**Fig. 9** Distribution of uncured adhesive layer after preheating pulse: **a** preheating time of 100 ms; **b** preheating time of 200 ms
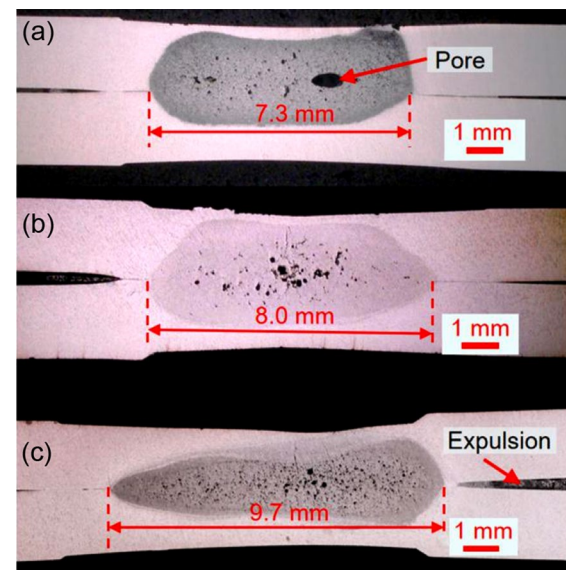


**Fig. 10** Cross-sectioned morphologies of the weld-bonded joints: **a** WB-I; **b** WB-II; **c** WB-III
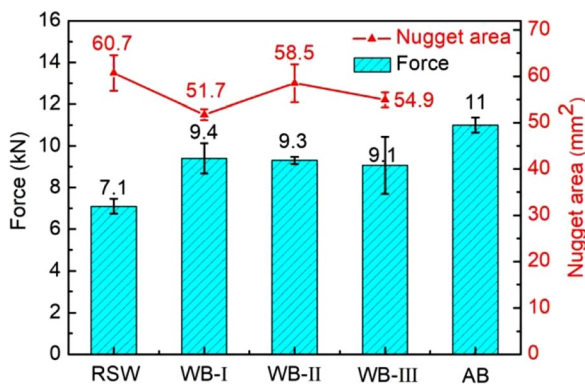
**Fig. 11** Nugget areas and tensile shear forces of different joints

a higher resistance and a higher heat input and resulted in a larger growth rate of the nugget and a larger penetration [20, 27]. Therefore, the WB-II joint has a larger nugget size and penetration than the WB-I joint. However, excessive heat led to severe expulsion, resulting in loss of molten metal and larger indentation, causing larger heat dissipation rate through cooling water, resulting in the smallest nugget penetration (refer to Fig. 10c).

Figure 11 compares the nugget area and tensile shear forces of RSW, WB and adhesive bonding (AB) joints under the optimized welding parameters. RSW nugget has the largest nugget area, followed by WB-II, WB-III, and WB-I. After optimizing the parameters, the adhesive effect of removing welding spot area was improved by using an electrode force of 5.5 kN, which reduces the contact resistance between W/W and thus reduces the current density and the resistance heat. As a result, the nugget area of WB-I was only 51.7 mm$^2$. The nugget size of WB-II was increased to 58.5 mm$^2$, close to the RSW nugget size, which resulted from the increased total heat input during welding through adding the preheating pulse. However, the overheat input at preheating time of 200 ms caused expulsion, resulting in the loss of nugget metal, causing the smaller nugget area of WB-III joint compared to that of the WB-II joint.

For tensile shear loads, the RSW joint had a minimum load of 7.1 kN, while adhesive joint owned a maximum load of 11.0 kN. The weld-bonded joints achieved the strength that is larger than the RSW joints but smaller than the adhesive joints. The introduction of the adhesive increased the bonding area of the WB joints, decreased the stress concentration in the WB joints [22], and contributed the WB joints to achieve higher strength. However, the expulsion during the WB process and the welding defects, e.g., gas pores, in the WB joints deteriorated joint strength, causing lower tensile shear loads than the AB joints.

Compared to WB joints with preheating pulse, the strength of WB-I joint is slightly higher than that of the WB-II and WB-III joints. Though the nugget area of the

WB-I joints was slightly smaller than that of the WB-II and WB-III joints, the nearly defects-free joints contributed the joints to withstand a larger tensile shear load. Compared to the WB-II joint, severe expulsion and carbonization of large area of the adhesive layer during welding is observed, deteriorating the strength of the WB-III joint and causing the lowest tensile shear force. In addition, compared to the WB-I and WB-III joints, the WB-II joint had the smallest standard deviation of the tensile shear force, indicating that the performance of WB-II joint is more stable after preheating of 100 ms under 10 kA current.

## 5 Conclusions

In this paper, the effects of the process parameters on the weld-bonded nugget area and tensile shear strength are studied based on the orthogonal experiments. To improve the strength of WB joints of 5754 aluminum alloy, the WB process was optimized. The following conclusions can be drawn:

1. The welding parameters have significant effects on the nugget area. And the welding current has the largest significance, followed by the welding time, and then the welding pressure. In addition, the welding parameters have a nonlinear influence on the mechanical properties of the weld-bonded joints.
2. It is difficult to obtain stable mechanical properties using WB process for 5754 aluminum alloy, caused by the residual adhesive at the welding zone and thus the instable contact state between workpieces. The residual adhesive layer leads to a large and unstable contact resistance, easily causing expulsion during welding and thus destroying the integrity of the weld nugget and the adhesive layer, weakening joint strength.
3. A larger nugget size and fewer welding defects are achieved using the optimized welding parameters. The nugget size and quality are further improved by adding a preheating pulse with a preheating current of 10 kA and preheating time of 100 ms, and the stability of joint performance is also improved.

## Compliance with Ethical Standards

**Conflict of interest** On behalf of all the authors, the corresponding author states that there is no conflict of interest.

# References

1. Meschut, G., Janzen, V., Olfermann, T.: Innovative and highly productive joining technologies for multi-material lightweight car body structures. J. Mater. Eng. Perform. **23**(5), 1515–1523 (2014)
2. Han, L., Thornton, M., Boomer, D., et al.: A correlation study of mechanical strength of resistance spot welding of AA5754 aluminium alloy. J. Mater. Process. Technol. **211**(3), 513–521 (2011)
3. Li, M., Zhu, Z., Xiao, Q., et al.: Mechanical properties and microstructure evolution of dissimilar Mg and Al alloys welded using ultrasonic spot welding. Mater. Res. Express. **6**(8), 086588 (2019)
4. Deng, L., Li, Y.B., Carlson, B.E., et al.: Effects of electrode surface topography on aluminum resistance spot welding. Weld. J. **97**(4), 120s–132s (2018)
5. Florea, R.S., Solanki, K.N., Bammann, D.J., et al.: Resistance spot welding of 6061-T6 aluminum: failure loads and deformation. Mater. Des. **34**, 624–630 (2012)
6. Li, Y.B., Wei, Z.Y., Wang, Z.Z., et al.: Friction self-piercing riveting of aluminum alloy AA6061-T6 to magnesium alloy AZ31B. J. Eng. Ind. **135**(6), 061007 (2013)
7. Zhang, W.J., Cross, I., Feldman, P., et al.: Electrode life of aluminium resistance spot welding in automotive applications: a survey. Sci. Technol. Weld. Join. **22**(1), 22–40 (2017)
8. Ferreira, A.C., Campanelli, L.C., Suhuddin, U.F.H., et al.: Investigation of internal defects and premature fracture of dissimilar refill friction stir spot welds of AA5754 and AA6061. Int. J. Adv. Manuf. Technol. **106**(3), 3523–3531 (2020)
9. Hayat, F.: Effect of aging treatment on the microstructure and mechanical properties of the similar and dissimilar 6061-T6/7075-T651 RSW joints. Mater. Sci. Eng. A **556**, 834–843 (2012)
10. Min, J., Li, J., Li, Y., et al.: Friction stir blind riveting for aluminum alloy sheets. J. Mater. Process. Technol. **215**(215), 20–29 (2015)
11. Feng, Q.B., Li, Y.B., Carlson, B.E., et al.: Study of resistance spot weldability of a new stainless steel. Sci. Technol. Weld. Join. **24**(2), 101–111 (2019)
12. Wan, Z., Wang, H.P., Wang, M., et al.: Numerical simulation of resistance spot welding of Al to zinc-coated steel with improved representation of contact interactions. Int. J. Heat Mass Transf. **101**, 749–763 (2016)
13. Florea, R.S., Bammann, D.J., Yeldell, A., et al.: Welding parameters influence on fatigue life and microstructure in resistance spot welding of 6061-T6 aluminum alloy. Mater. Des. **45**, 456–465 (2013)
14. Manladan, S.M., Yusof, F., Ramesh, S., et al.: A review on resistance spot welding of aluminum alloys. Int. J. Adv. Manuf. Technol. **90**(1–4), 605–634 (2017)
15. Darwish, S.M., Al-Samhan, A.M.: Peel and shear strength of spot-welded and weld-bonded dissimilar thickness joints. J. Mater. Process. Technol. **147**(1), 51–59 (2004)
16. Barnes, T.A., Pashby, I.R.: Joining techniques for aluminium spaceframes used in automobiles: part II—adhesive bonding and mechanical fasteners. J. Mater. Process. Technol. **99**(1–3), 72–79 (2000)
17. Costa, H.R.M., Reis, J.M.L., Souza, J.P.B., et al.: Experimental investigation of the mechanical behaviour of spot welding–adhesives joints. Compos. Struct. **133**, 847–852 (2015)
18. Chang, B.H., Shi, Y.W., Dong, S.J.: A study on the role of adhesives in weld-bonded joints. Weld. J. **78**, 275–279 (1999)
19. Weber, G., Thommes, H., Gaul, H., et al.: Resistance spot welding and weldbonding of advanced high strength steels. Materialwiss. Werkstofftech. **41**(11), 931–939 (2010)
20. Zhang, Y.S., Sun, H.T., Chen, G.L., et al.: Comparison of mechanical properties and microstructure of weld nugget between weld-bonded and spot-welded dual-phase steel. Proc. Inst. Mech. Eng. Part B **223**(10), 1341–1350 (2009)
21. Goncalves, V.M., Martins, P.A.F.: Static and fatigue performance of weld-bonded stainless steel joints. Mater. Manuf. Process. **21**(8), 774–778 (2006)
22. Pouranvari, M., Safikhani, E.: Mechanical properties of martensitic stainless steel weld/adhesive hybrid bonds. Sci. Technol. Weld. Join. **23**(3), 227–233 (2018)
23. Xia, Y., Zhou, Q., Wang, P.C., et al.: Development of high-efficiency modeling technique for weld-bonded steel joints in vehicle structures—part I: static experiments and simulations. Int. J. Adhes. Adhes. **29**(4), 414–426 (2009)
24. Sam, S., Shome, M.: Static and fatigue performance of weld bonded dual phase steel sheets. Sci. Technol. Weld. Join. **15**(3), 242–247 (2010)
25. Zhang, Y., Shen, J., Zhao, Y., et al.: Effect of adhesive characteristics on the weld quality in weld bonding multiple steel sheets. Weld. J. **92**(12), 303s–374s (2013)
26. Han, L., Thornton, M., Boomer, D., et al.: Effect of aluminium sheet surface conditions on feasibility and quality of resistance spot welding. J. Mater. Process. Technol. **210**(8), 1076–1082 (2010)
27. Khan, M.D.F., Sharma, G., Dwivedi, D.K.: Weld-bonding of 6061 aluminium alloy. Int. J. Adv. Manuf. Technol. **78**(5–8), 863–873 (2015)
28. Khan, M.D.F., Dwivedi, D.K.: Mechanical and metallurgical behavior of weld-bonds of 6061 aluminum alloy. Mater. Manuf. Process. **27**(6), 670–675 (2012)
29. Khan, M.D.F., Dwivedi, D.K., Sharma, S.: Development of response surface model for tensile shear strength of weld-bonds of aluminium alloy 6061 T651. Mater. Des. **34**, 673–678 (2012)
30. Pereira, A.M., Ferreira, J.A.M., Antunes, F.V., et al.: Assessment of the fatigue life of aluminium spot-welded and weld-bonded joints. J. Adhes. Sci. Technol. **28**(14–15), 1432–1450 (2014)
31. Liu, A., Tang, X., Lu, F.: Study on welding process and prosperities of AA5754 Al-alloy welded by double pulsed gas metal arc welding. Mater. Des. **50**, 149–155 (2013)
32. Datta, S., Bandyopadhyay, A., Pal, P.K.: Application of Taguchi philosophy for parametric optimization of bead geometry and HAZ width in submerged arc welding using a mixture of fresh flux and fused flux. Int. J. Adv. Manuf. Technol. **36**(7–8), 689–698 (2008)
33. Datta, S., Bandyopadhyay, A., Pal, P.K.: Grey-based Taguchi method for optimization of bead geometry in submerged arc bead-on-plate welding. Int. J. Adv. Manuf. Technol. **39**(11–12), 1136–1143 (2008)
34. Lin, J., Hua, D., Wang, P.C., et al.: Effect of thermal exposure on the strength of adhesive-bonded low carbon steel. Int. J. Adhes. Adhes. **43**, 70–80 (2013)
35. Rashid, M., Medley, J.B., Zhou, Y.: Electrode worksheet interface behaviour during resistance spot welding of Al alloy 5182. Sci. Technol. Weld. Join. **14**(4), 295–304 (2009)
36. Ashiri, R., Mostaan, H., Park, Y.D.: A phenomenological study of weld discontinuities and defects in resistance spot welding of advanced high strength TRIP steel. Metall. Mater. Trans. A **49**(12), 6161–6172 (2018)
37. Sun, X., Stephens, E.V., Khaleel, M.A.: Effects of fusion zone size and failure mode on peak load and energy absorption of advanced

high strength steel spot welds under lap shear loading conditions. Eng. Fail. Anal. **15**(4), 356–367 (2008)

38. Wang, S., Min, J., Lin, J., et al.: Effect of atmospheric pressure plasma treatment on the lap-shear strength of adhesive-bonded sheet molding compound joints. Automot. Innov. **1**(3), 237–246 (2018)

39. Wan, H., Lin, J., Min, J.: Effect of laser ablation treatment on corrosion resistance of adhesive-bonded Al alloy joints. Surf. Coat. Technol. **345**, 13–21 (2018)

40. Bartczak, B., Mucha, J., Trzepiecinski, T.: Stress distribution in adhesively-bonded joints and the loading capacity of hybrid joints of car body steels for the automotive industry. Int. J. Adhes. Adhes. **45**, 42–52 (2013)